Opto-Mechanical Design of the Wide-Field Infrared Transient Explorer (WINTER) Fly's Eye Camera

Erik Hinrichsen^a, Mark Egan^a, Nathan P. Lourie^a, Danielle Frostig^{a,b}, Gábor Fűrész^a, Robert Simcoe^{a,b}, and Andrew Malonis^a

^aMIT Kavli Institute for Astrophysics and Space Research, 77 Mass. Ave, Cambridge, MA 02139, USA

^bMIT Department of Physics, 77 Massachusetts Ave., Cambridge, MA 02139, USA

ABSTRACT

The Wide-Field Infrared Transient Explorer (WINTER) is a new infrared time-domain survey instrument on a dedicated 1 meter robotic telescope at the Palomar Observatory. WINTER will perform the first seeing-limited time domain survey of the infrared (IR) sky, with a particular emphasis on identifying r-process material in binary neutron star (BNS) merger remnants detected by LIGO. We have developed and tested a custom optomechanical mounting scheme for a 6-channel tiled optical system with >90% fill factor. Here, we present the mechanical design and testing approach used in the development of WINTER.

Keywords: WINTER, Lens Array Mounting, Adhesive lens mounting

1. INTRODUCTION

The Wide-Field Infrared Transient Explorer (WINTER) is a new infrared instrument that will be installed on a dedicated 1 meter robotic telescope at the Palomar Observatory. Commissioning is planned for mid-2021. In this paper, we describe the mechanical design implementation of WINTER, with a particular focus on the opto-mechanical design of the lens mounts. This paper is published along with companion papers describing an overview of WINTER, ¹ the design requirements and validation, ² and the detector architecture. ³

In Section 2, we give a brief overview of the WINTER optical design. The custom camera optics developed for WINTER result in >90% fill factor in a 1° x 1° square field of view, while using a non-abutting array of InGaAs detectors. In Section 3, we present the results of extensive bond strength testing. This was undertaken to validate our bonding methods and bond design prior to proceeding with detailed mounting designs. In Section 4, we describe the lens mount designs and validation testing. The lens mounts are of two types; the first is a bonded flexure mount allowing precision adjustment in a single axis. This design required careful attention to bonding fixtures and mechanical tolerances to satisfy the optical design requirements. The second lens mount type includes 5 axis adjustment (3 linear, 2 angular) using several types of custom-designed flexure stages.

2. OPTICAL DESIGN OVERVIEW

The WINTER optical design is shown in overview in Fig. 1. The optics consist of a filter array, field lens array, fold mirror, and 6 identical optical trains (3 per side). The field lenses are bonded edgewise into a 3 x 2 rectangular array placed near the telescope focus, which divides the telescope beam into 6 channels with >90% fill factor. The lens elements are truncated symmetrically about one plane in order to fit the closely packed optical design. With the exception of the Lens 6-7 doublet, the lenses are bonded side by side such that 3 channels form a single tiled element, hereafter referred as the "tiled lens elements." The design requires that the truncating operation be extremely precise; the cut edges are required to be perpendicular to the rear flat to within 4 µm and symmetric about the center plane to within 10 µm. The lens 6-7 doublets meanwhile require independent adjustment, and thus are not bonded into tiles. We refer to these elements as "compensator lens elements".

Further author information: send correspondence to Erik Hinrichsen at ehinrich@mit.edu

Ground-based and Airborne Instrumentation for Astronomy VIII, edited by Christopher J. Evans, Julia J. Bryant, Kentaro Motohara, Proc. of SPIE Vol. 11447, 114479F · © 2020 SPIE · CCC code: 0277-786X/20/\$21 · doi: 10.1117/12.2562912

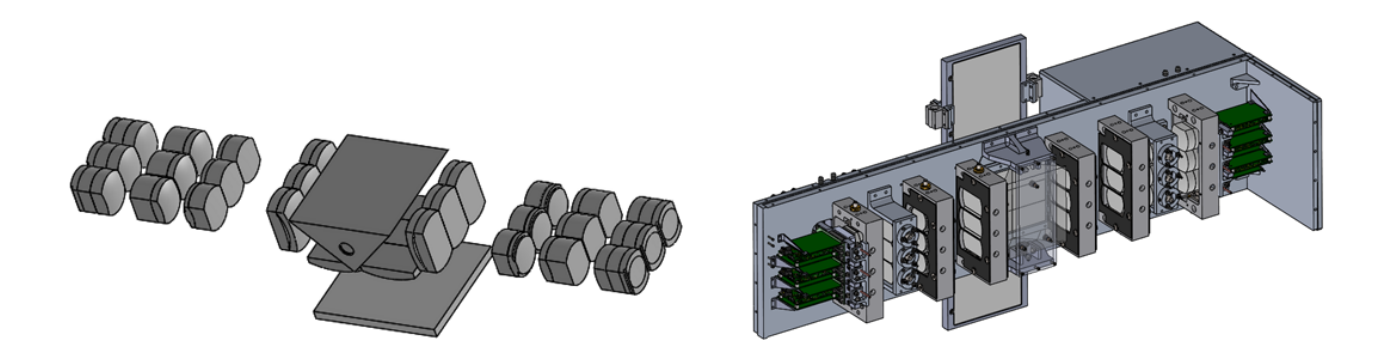


Figure 1. Left: Isometric view of the WINTER optics. Note that only 1 of 3 filters is shown; Right: Instrument view with covers removed

At the focus of each channel is an InGaAs detector. These large format commercial detectors are cooled with a simple in-package thermo-electric cooler (TEC) connected to a heat sink, with significant implications for the mechanical design of WINTER. This allows the remainder of the instrument to reside at ambient temperatures.

The WINTER instrument will be installed on a modified PlaneWave Industries PW1000 telescope. The telescope has custom mirror coatings and a secondary mirror focuser designed by PlaneWave for WINTER.

3. BOND DESIGN AND TESTING

The highly compact, tightly packed optical design of WINTER made adhesive bonding an attractive option for lens mounting. Adhesive bonding presents several important advantages over mechanical clamping – among them being reduced mass, reduced mechanical complexity, and potentially reduced stress into the optics.

However, adhesive bonding is highly process dependent. Adhesive choice, bond design, surface preparation, and curing schedule all have significant effects on resulting bond quality. Environmental exposure can result in significant thermal stress and aging of the adhesive. Although every effort has been made to account for these issues in the design, physical testing is irreplaceable. Therefore, we conducted extensive bond strength tests before proceeding to detailed mechanical design.

3.1 Adhesive bonding tests

The purpose of the bonding tests is to validate the bond design against the system requirements. WINTER is designed for a 10 year life span; ambient temperatures ranging from -7 to 34 °C; and shipping loads as high as 6g. In this section, we will describe how we designed the bond to meet these requirements and present the results of our validation tests.

We initially studied a number of candidate adhesives. As a basis for study, we selected an 11 mm bond diameter, which provided a substantial strength safety factor for all candidates based on tensile strength and expected loads. We evaluated candidates by calculating thermal shear stress at 40° C and -10° C using the approach described by Yoder and Vukobratovich.⁴ This range is slightly outside historical norms at Palomar, which ranged from -7 to 34 °C over the past 10 years. Based on these results, we selected 3M Scotch-Weld 2216 A/B Gray epoxy. This epoxy is well characterized, with easily available material properties.⁵ It has the lowest calculated thermal stress of the candidate adhesives, readily cures at room temperature, does not present outgassing hazards, and bonds well to a variety of metals and glasses.

Next, we conducted a double lap shear test to validate the bond strength against published values.⁵ This test used a glass tab sandwiched between 2 metal tabs (see Fig. 2). The metal tab material was Grade 410 stainless steel, chosen for its corrosion resistance and good thermal expansion match with the WINTER lens materials. The glass material was Ohara S-LAL14, the WINTER glass with the greatest thermal expansion difference with SS410 (5.7 ppm/C vs. 9.9 ppm/C). A 0.22 mm deep channel was machined into the metal tabs to set the bond thickness, with a 1.02 mm diameter adhesive injection hole in the center. The bonding surface was uniformly

roughened to between 3.2 and 6.3 μ m average surface roughness. The surface of the glass tabs was roughened to 400 grit finish (approximately 0.23 μ m R_a).

Prior to bonding, the metal tabs were cleaned with acetone, then a thin layer of Solvay BR 127 corrosion-inhibiting primer was applied a brush. The primer was left to dry at room temperature for 30 minutes, then cured at 82 °C for 4 hours. Immediately before bonding, the glass was cleaned with acetone, then primed with a thin layer of 3M EC-3901 Structural Adhesive Primer. The test pieces were assembled on a fixture with Kapton polyimide tape applied to maintain contact pressure between substrates. The 2216 A/B was mixed by hand and then outgassed in a vacuum bell jar for 10 minutes before dispensing. A pneumatic dispenser was used to inject adhesive through the dispensing holes in the tabs; a visual target was used to evaluate bond diameter. The samples were then left to cure at room temperature for at least 7 days. We prepared 9 test pieces using a single batch of adhesive.

The prepared test pieces were evenly split into 3 testing regimes. A control group remained in a clean room until testing. A thermal cycling group underwent 100 cycles between -10 and 40 °C with a 10 minute rise time and a 30 minute soak. The predicted thermal shear stresses at these temperatures are -0.70 and 0.36 MPa, respectively. Finally, a humidity aging group was placed in an oven at 65 °C with open water containers to increase humidity for 7 days, then conditioned at room temperature for 7 days. Average relative humidity in the oven was 49%.

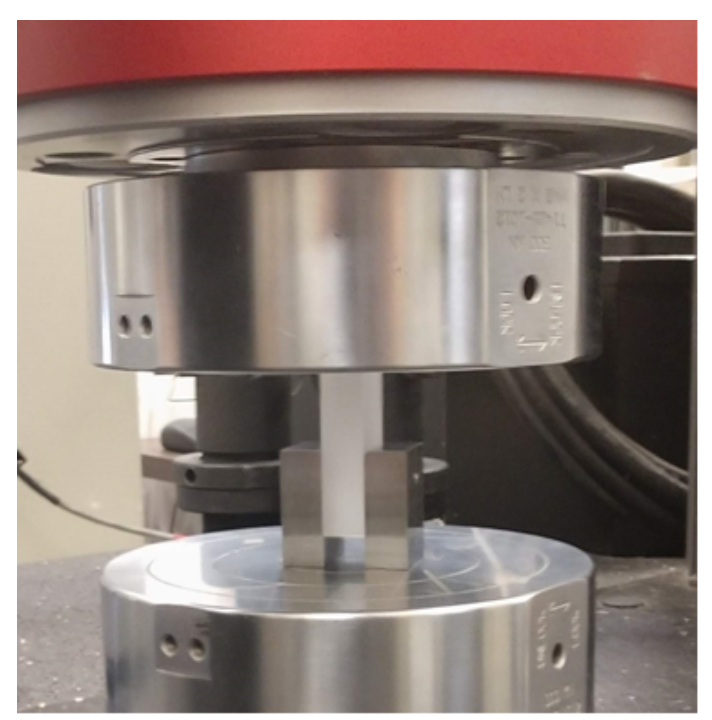
The specimens were tested on an Instron 5984 Universal Testing Machine. They were tested in compression at a rate of 1.27 mm/min until failure. The results are shown in Fig. 3 and tabulated in Table 1. No deleterious effects were seen in the environmentally tested samples. Ultimate shear stress was calculated by dividing failure load by bond area. These values were lower than published overlap shear strength values (3200 PSI⁵), although no published values are available for metal to glass bonds. The test results are acceptable for WINTER's application.

Testing Regime	Mean Ultimate Load (lbf)	Mean Ultimate Stress (PSI)	
Control	681.0	2312	
Thermal Cycling	746.9	2532	
Humidity Aging	853.2	2896	

Table 1. Adhesive double lap shear test results

A second test was conducted using a mock-up of a lens mounting tab concept. This was done to characterize the cleavage strength, which is more relevant than lap shear strength for the loads experienced in WINTER. Again, two mounting tabs were fabricated out of Grade 410 stainless steel. The mounting face is milled to a cylindrical surface of radius 21 mm with a recessed face of radius 21.22 mm. The recessed face is uniformly roughened to $3.2 - 6.3 \,\mu m$ R_a. There is a central 1.02 mm diameter hole for adhesive injection. A cylindrical glass piece made from OHARA S-LAL14 with 42 mm diameter has its outer edge roughened to 400 grit. Refer to Fig.2 for images of the mock-up assembly and bonding fixture. Nine samples were prepared according to the bonding and curing procedures described in the lap shear test. After curing, 5 samples were taken as controls and 4 were subjected to thermal cycling tests. Humidity aging was not conducted due to time constraints.

The bonded pieces were tested on an Instron 5984 machine using a 3 point bending fixture. They were tested in compression at a rate of 1.27 mm/min. The test results are shown in Fig.4. The minimum required failure load was calculated as 10.15 lbf, based on a 5g acceleration load and a safety factor of 3. This is drawn with a red line in the image. As the test results show, the bond strength is significantly higher than required, and again shows no deterioration with thermal cycling.







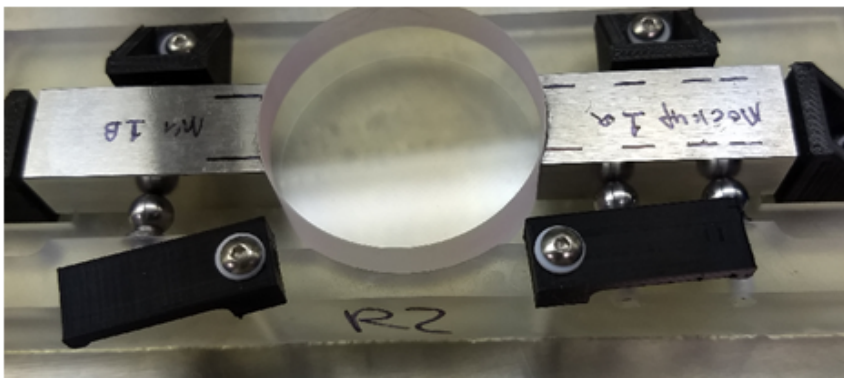


Figure 2. WINTER bond testing. Clockwise from top left: lap shear testing; 3 point bend testing of lens mock-up; lens mock-up in bonding fixture; lap shear sample after failure.

4. MECHANICAL DESIGN IMPLEMENTATION

4.1 Tiled lens mounting

The tiled lens mount design was driven by the lens positioning requirements as shown in Table 2. In order to minimize complexity during system alignment, a lens mount was designed which is adjustable in a single axis. The remaining requirements are achieved through a combination of mechanical tolerances and careful adjustment prior to bonding.

4.1.1 Design

The mount design consists of two flexure lens mounts bolted into a rectangular frame. The flexure lens mounts each have 2 adhesive injection holes, allowing bonding to the truncated edges of the tiled lens element. A 100 thread per inch adjustment screw is installed on one side, enabling lateral adjustment to approximately 1 micron precision.

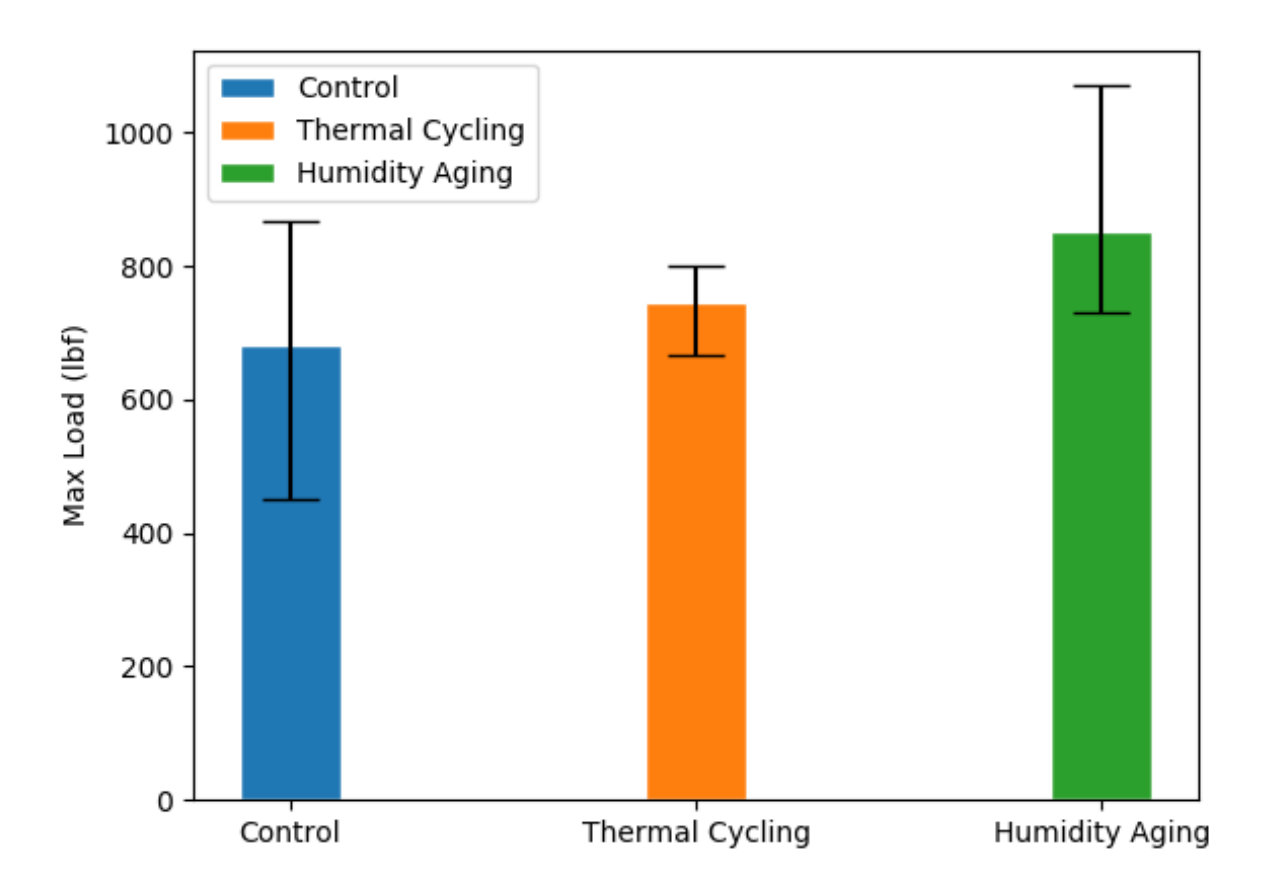


Figure 3. Double lap shear bond testing failure loads. The error bars show the maximum and minimum recorded values.

The frame material is MIC-6 aluminum, a cast metal with low residual stress. This low stress state aids in maintaining tight precision requirements while removing large amounts of material during machining. As the optical bench material is also aluminum, this prevents thermal expansion distortions from developing.

The flexure mounts are made from Titanium 6Al-4V, which in this case has several advantages over the Grade 410 stainless steel used in our bonding tests. Ti 6Al-4V was chosen on the basis of its high yield strength, good corrosion resistance, and good thermal expansion match with the lens materials. Though this constitutes a change from the conditions of the bond test, tests with Ti 6Al-4V and 2216 A/B epoxy have shown comparable results with our bonding tests. The flexure interfaces with the lens edge as shown in Fig. 5. A conical feature is machined into the flexure bonding face; a stainless steel ball with one face ground flat sits in the conical recess. Because the balls are free to rotate, the interface is defined by the truncated lens edge without over-constraint. The cone depth and ball height define a 0.22 mm bond thickness.

The flexure design supports a maximum lateral adjustment of 0.5 mm. The flexures take the form of two 1 mm thick rectangular beams meeting at the center of the part, with a 0.75 mm relief machined using wire electrical discharge machining (EDM). The lens frames are offset 0.25 mm when mounted to allow symmetrical adjustment. The flexures were designed using finite element analysis (FEA) such that maximum stress is less than one third of yield stress. The analysis shows a bending stress of 265 MPa, which is less than one-third of the yield stress (827 MPa), a typical criterion for flexure design. To validate the FEA results, we used the analytical approach described by Smith and Chetwynd, with an additional stress concentration factor for the

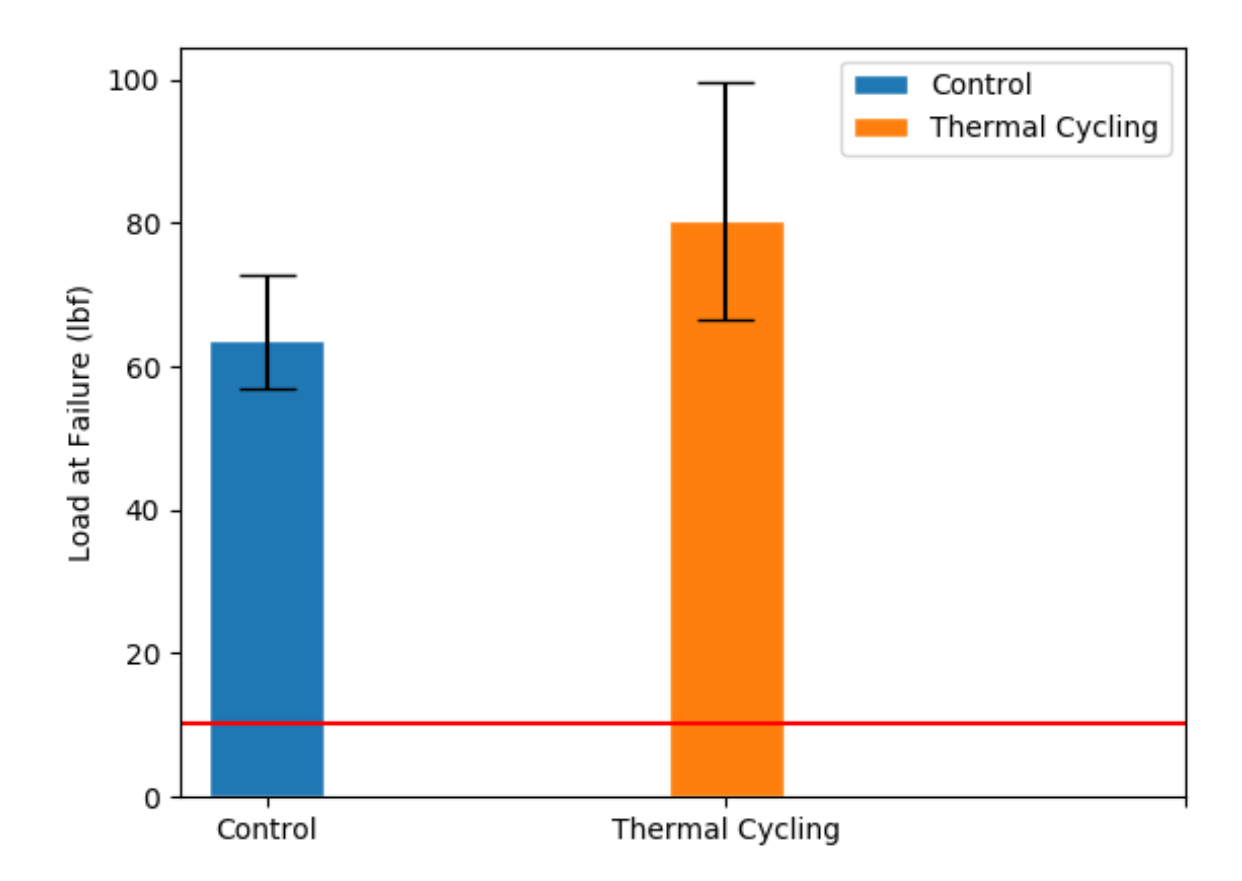


Figure 4. Mock-up bonding results. The horizontal red line is the requirement.

interior fillet. The resulting equation is given as follows:

$$\sigma_{max} = \frac{3K_t q_{max} Ed}{L^2} \,, \tag{1}$$

where q_{max} is maximum displacement; K_t is the stress concentration factor; σ_{max} is maximum bending stress; L is the flexure length; E is Young's modulus; and d is flexure thickness. K_t is found to be 1.3 from a chart of stress concentration factors for rectangular filleted bars in bending. For a displacement of 0.5 mm, this equation gives a stress of 264 MPa, which is within 1% of the FEA value.

4.1.2 Assembly and testing

Because the tiled lens mount has fine adjustment in a single axis, the remaining degrees of freedom must be precisely aligned in during assembly. This is accomplished through mechanical tolerancing and careful prebonding alignment.

The basis for accurate leveling is a custom granite surface plate with inspection grade A flatness (3.81 μ m over 46 cm x 610 cm) made by Rock of Ages. An array of threaded inserts installed installed for mounting the lens frames and a Hexagon Absolute Series coordinate measuring machine (CMM) arm. The CMM arm has \sim 25 μ m single point measurement accuracy. To minimize clamping distortion, the rear face of the lens frame has a 0.0127 mm flatness tolerance. The lens array is placed on 3 evenly spaced commercial grade 0 gauge blocks

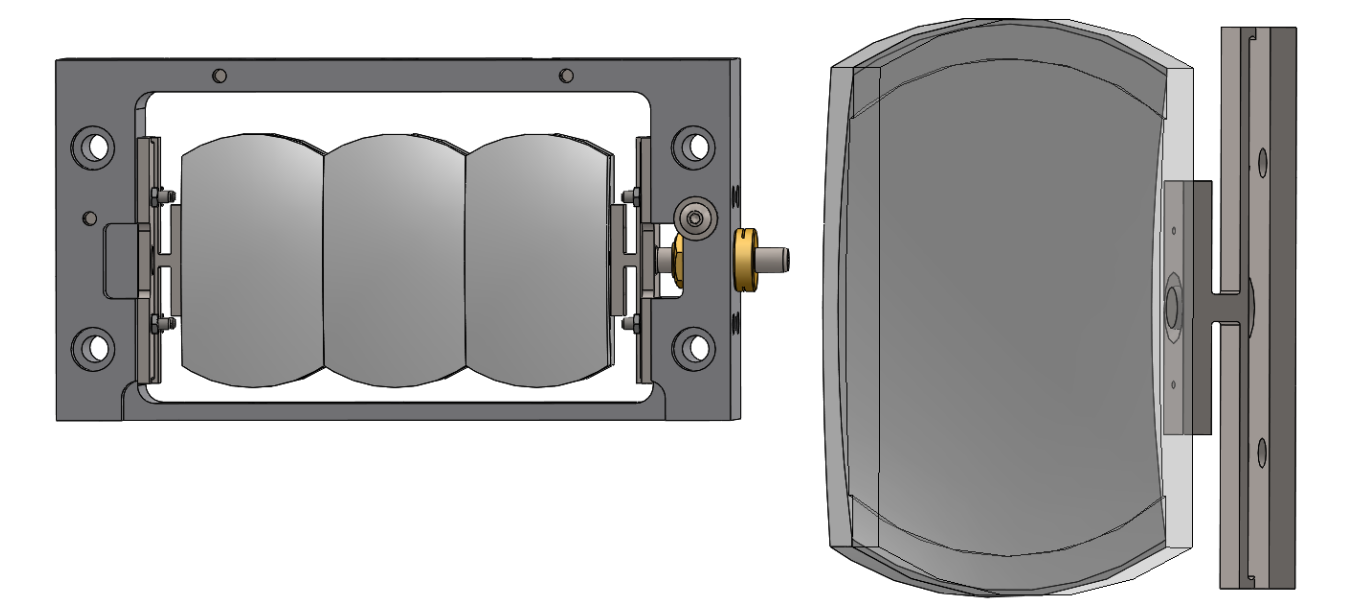


Figure 5. Left: Tiled lens in frame mount assembly. Right: Flexure mount interface with lens, showing truncated ball face in cone.

(height tolerance $\pm 0.15 \,\mu\text{m}$), each with a thin plastic shim to protect the glass. The lens alignment is measured with the CMM arm prior to bonding, and may be adjusted by adding shims.

The lens height in the frame is adjusted from the top by a centered 100 thread-per-inch threaded adjuster. The opposing face has 3 holes for measuring the lens height and rotation. A Mitutoyo depth micrometer with 3 μ m accuracy was used for these measurements. Off-center adjustment screws are used to correct rotational misalignment of the tiled optic, as shown in Fig.5. The adjustment screws are removed after bonding.

A prototype was assembled to test the design, shown in Fig. 7. We fabricated two parts as stand-ins for the tiled optic: an aluminum block and an N-BK7 glass block. The aluminum block was used for validating alignment, as fabricating a single glass piece to the required tolerances was significantly more expensive. The glass piece was used for bond testing and verifying that the alignment procedure would not damage the lenses.

As shown in Table 2, we were able to align the test optic to the system requirements. Once the alignment was complete, we bonded the N-BK7 optic stand-in to the frame, using the same procedure as described in Sec. 3. The assembly was exposed to a thermal cycle test to verify survival at the site temperature extents. 50 cycles between 35 and -7 °C were completed. No damage to the bonds was observed. The assembly was re-measured and found to match the pre-bonding alignment.

4.2 Compensator lens mounting

A custom 5 axis adjustable mount was designed for the compensator lenses. The 6th degree of freedom, a rotation of the lens, is set during bonding. The need for a custom adjustable mount was driven by the compensator lens positioning tolerances (shown in Table 3) and the 36 mm inter-channel spacing.

Of the 5 adjustable axes, 3 are actively adjusted during system alignment. These are the lens height, tilt, and lateral position. The lens tip and position are set according to system tolerances. The design takes a stacked stage approach, in which each stage adjusts a single axis. The stages are separated by metal shims to prevent them from dragging. This approach consumes little area on the optical bench, and uses simple components which are relatively inexpensive. Each stage is aligned to the next with dowel pins mated to a hole and slot.

The three linear adjustment stages are formed from flexure beams machined into a metal block using wire EDM. The flexures are in opposition to each other, creating a stage which is compliant in the adjustable axis

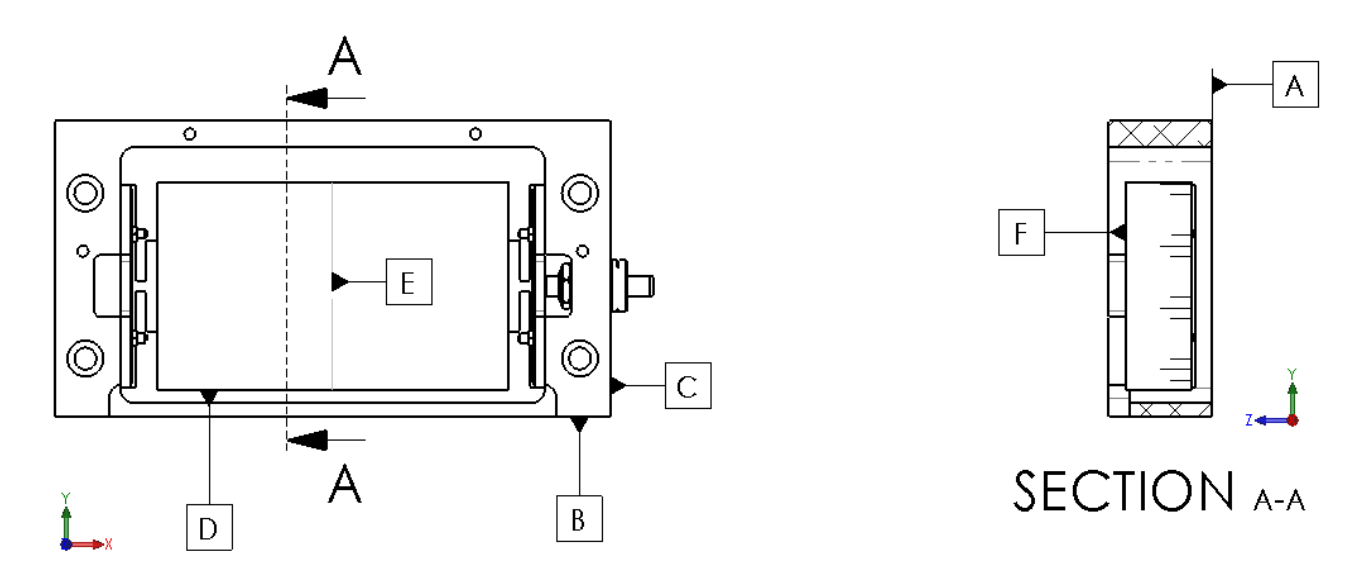


Figure 6. Labeled datums of test optic in frame for prototyping. Refer to Table 2 for measurements.

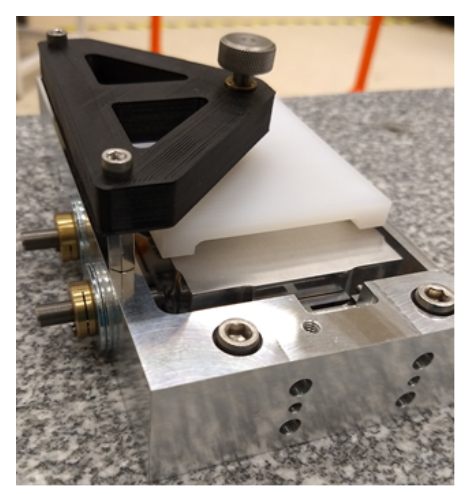
Dimension	Description	Nominal value	Tolerance	Measured value	Pass?
$R_{Z,DB}$	Rotation of optic about Z	0°	±0.02°	0.005°	Yes
$R_{X,FB}$	Rotation of optic about X	0°	±0.10°	0.057°	Yes
$R_{Y,FA}$	Rotation of optic about Y w/rt A	0°	±0.04°	0.001°	Yes
L_{DB}	Distance between datums A and B	8.25 mm	$\pm 0.025~\mathrm{mm}$	8.250 mm	Yes
L_{CE}	Distance between datums C and E	85.55 mm	$\pm 0.025 \text{ mm}$	85.552 mm	Yes

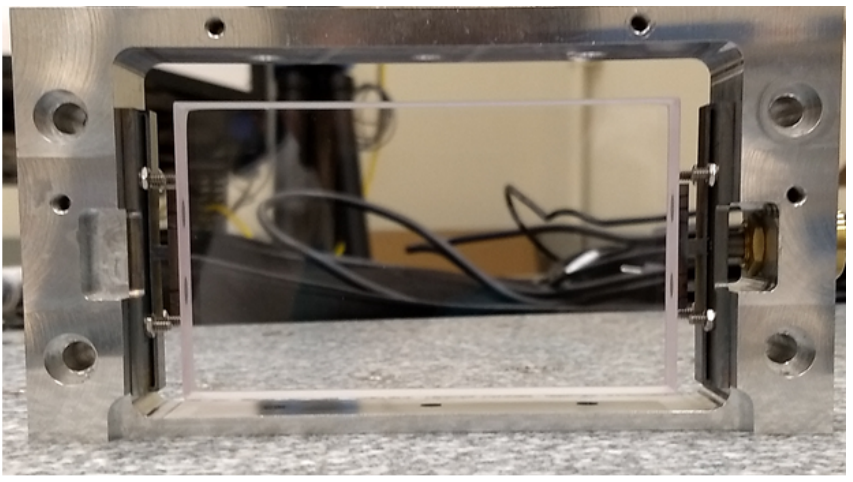
Table 2. Tiled Lens Requirements and Test Measurements

but very stiff out of axis. The flexures are adjusted with a 0.2 mm pitch adjustment screw, giving approximately $1.1~\mu m$ sensitivity. A spring plunger mounted opposite to the adjuster screw provides additional preload. The lens position and lateral stages are made from 7075-T6 aluminum, chosen for its high yield strength, low density, and matching thermal expansion with the lens frames. Consideration of thermal expansion is critical in order to maintain the height alignment with the tiled lenses. On the other hand, the lens height adjuster stage expands in opposition to the tiled lens frames, so it is made from Titanium 6Al-4V, a relatively low expansion material. The assembly is mounted on an aluminum block with sufficient height to take up the remaining expansion mismatch with the tiled lenses.

The two rotational adjustment stages are designed using circular flexure hinges. These have a center of rotation that is relatively invariant, ¹⁰ and are fairly simple to fabricate. We followed the classifications described by Yong, ¹⁰ which describes flexures as "thin," "intermediate," or "thick" based on the ratio of neck thickness to flexure radius. We selected a ratio in the intermediate regime, then used equations developed by Schotborgh ¹¹ — found by Yong to be accurate within 1.2% of FEA results — to design the flexures. The design criteria were stress below 1/3 of yield stress at 1° rotation, and actuation force lower than maximum for our selected actuator. We verified results using an FEA analysis which agreed with the analytical results within 3.4%. The lens tilt adjustment is off-axis from the lens, and thus exhibits cross-talk with lens position. Neither axis is adjusted during system alignment, so this is acceptable. Meanwhile, the lens rotation stage center of rotation is placed at the center of the lens axis of rotation to minimize cross-talk.

The compensator lenses are bonded to the tilt stage and a mounting tab using the same surface preparation





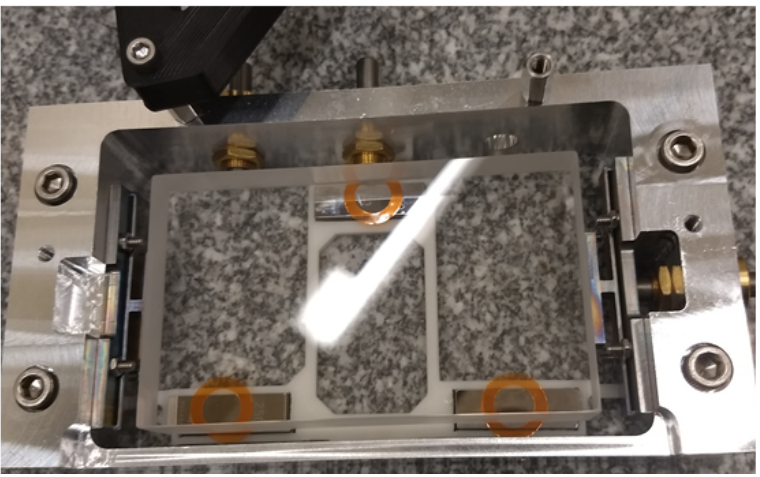


Figure 7. **Top left**: Tiled lens assembly with aluminum optic stand-in in bonding fixture; **Top right**: Bonded assembly with glass optic stand-in; **Bottom**: Assembly in bonding fixture, with gauge blocks and shims visible.

Table 3. Compensator lens positioning requirements

Lens height	±10 μm
Lens axial position	±10 μm
Lens lateral position	±10 μm
Lens tip	±0.05°
Lens tilt	±0.05°

and adhesive as described previously. Titanium 6Al-4V was chosen for both components for its good thermal expansion match with the lenses and low density. The mounting tab is held in place with a locking ring, which stabilized the lens as it rotates with the telescope. The ring has 3 equally spaced threaded holes, through which 2 ball-end set screws and 1 ball-end spring plunger are mounted. The height adjustment stage has locking bars to stabilize the lens height, visible in Fig. 8.

We fabricated a prototype compensator lens assembly in order to validate the design. We also fabricated a

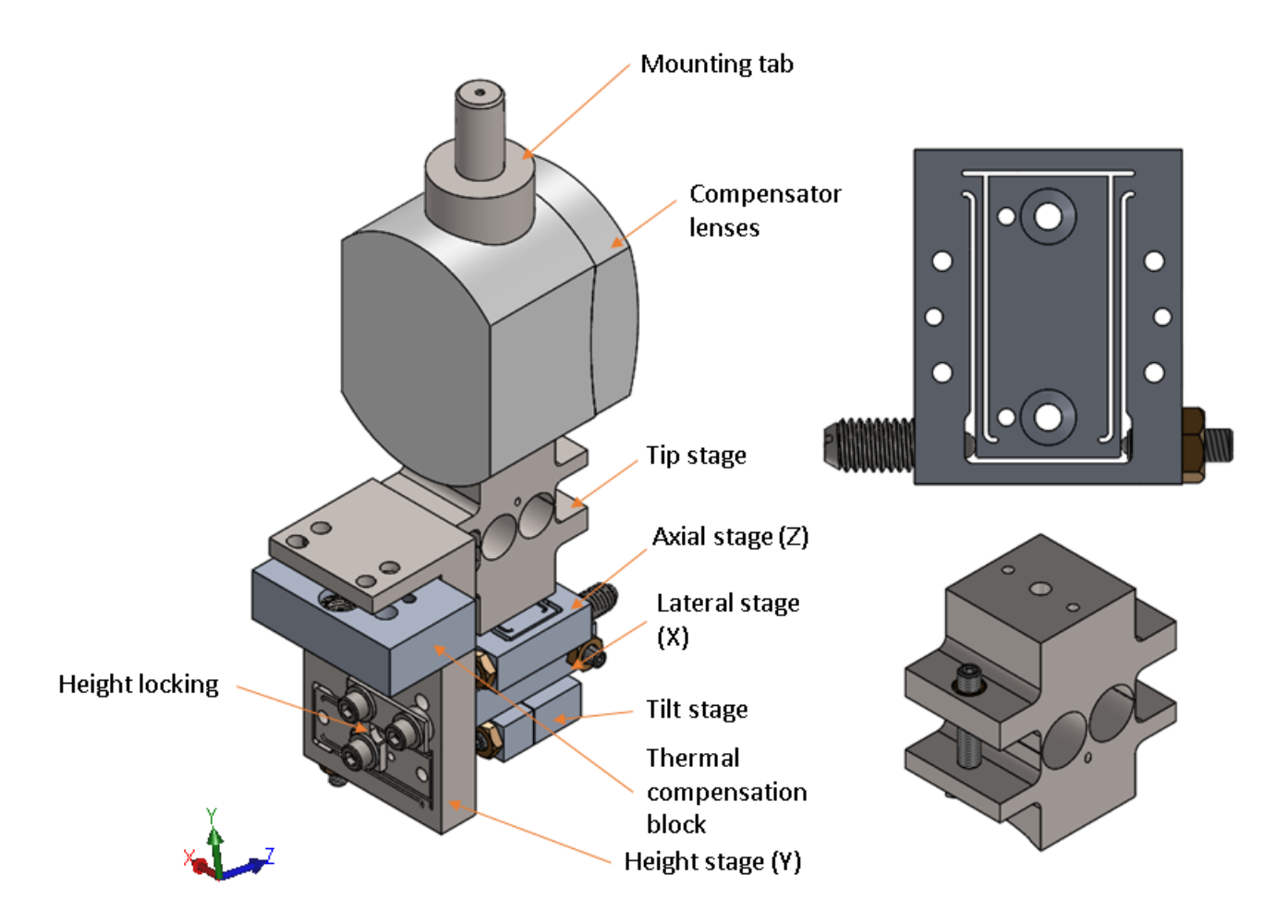


Figure 8. Left: Isometric view of compensator lens assembly; Top right: Linear flexure stage; Bottom right: Rotational flexure stage

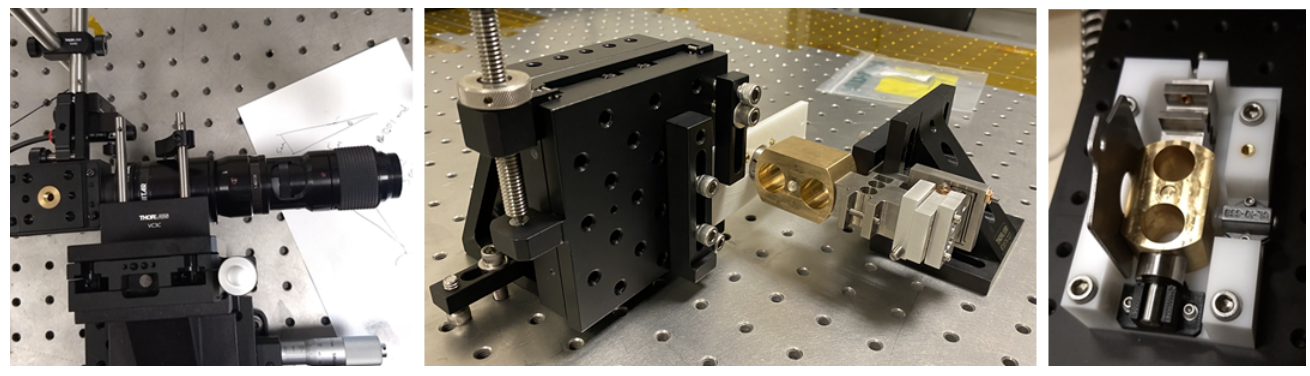


Figure 9. Left: Camera mounted on micrometer stage; Center: mounted compensator test assembly; Right: Compensator in bonding fixture.

bonding fixture, shown in Fig 9. We substituted a machined brass part with equivalent mass in place of the lenses. Once assembled, the compensator prototype was mounted on an optical bench along with a camera with lens. The camera was mounted on a 2 axis micrometer mount, allowing us to make precise adjustments to quantify cross-talk, locking effect, and minimum movement size. We captured images before and after making

calibrations, then used the *Register Virtual Slices* plug-in in Fiji¹²/ImageJ¹³ to determine the deviations between images. The camera was aligned with the compensator assembly with the help of a CMM arm.

The results are presented in Table 4 . We found generally low cross-talk with better than 10:1 ratio, although one axis had a 5:1 cross-talk ratio resulting from low stiffness of a 3D printed test fixture. Further effort is required to characterize the effect of locking the lens height, again owing to the test fixture limitations, as well as the tip and tilt effects. The minimum movement was found to be better than 2 μ m.

Table 4. Compensator lens test measurements

Description	X (mm/mm)	Y (mm/mm)	Ratio (active/cross-talk)	Movement (X) (µm)	Movement (Y) (µm)
Lateral position (X)	0.980	0.192	5.10		
Height (Y)	0.998	0.032	31.6		
Axial position (Z)	0.045	-0.100	22.2, -10.0		
Height Locking (Y)				6	-2
Stabilizer locking				49	5

4.3 Next steps

The major ongoing mechanical design efforts are on the detector cooling system and filter stage assembly. WINTER design efforts are expected to be complete by late spring 2021, and on-sky commissioning is planned for summer 2021.

ACKNOWLEDGMENTS

WINTER's construction is made possible by the National Science Foundation under MRI grant number AST-1828470. We also acknowledge significant support from the California Institute of Technology, the Caltech Optical Observatories (COO), the Bruno Rossi Fund of the MIT Kavli Institute for Astrophysics and Space Research, and the MIT Department of Physics and School of Science. Mike Martucci and Steven Powers of Optimax Systems, Inc. made significant contributions to the lens tile design.

REFERENCES

- [1] Lourie, N. P. and the WINTER Collaboration, "The wide-field infrared transient explorer (WINTER)," in [Proceedings of the SPIE], 11447(55) (2020).
- [2] Frostig, D. and The WINTER Collaboration, "Design requirements and performance validation for the wide-field infrared transient explorer (WINTER)," in [Proceedings of the SPIE], 11447(113) (2020).
- [3] Malonis, A. and The WINTER Collaboration, "Detector architecture of the wide-field infrared transient explorer (WINTER) InGaAs camera," in [Proceedings of the SPIE], 11454(105) (2020).
- [4] Yoder, P. and Vukobratovich, D., "Shear stresses in cemented and bonded optics due to temperature changes," in [Optomechanical Engineering 2015], Hatheway, A. E., ed., 9573, 141 148, SPIE (2015).
- [5] "3M Scotch-Weld™ Epoxy Adhesive 2216 B/A." https://multimedia.3m.com/mws/media/1539550/ 3mtm-scotch-weldtm-epoxy-adhesive-2216-b-a.pdf (October 2018). (Accessed 13 November 2020).
- [6] [Metallic Materials Properties Development and Standardization (MMPDS): Scientific Report (DOT/FAA/Ar-MMPDS-01)], Office of Aviation Research, Washington, DC (2003).
- [7] Massey, L., Werner, B., Banga, D., and Abelow, A., "Ideal surface conditions for titanium adhesion." https://www.osti.gov/biblio/1529205 (June 2018). (Accessed: 13 November 2020).
- [8] Smith, S. T. and Chetwynd, D. G., [Foundations of Ultra-Precision Mechanism Design], 100 103, CRC Press (September 2003).
- [9] Budynas, R. and Nisbett, J. K., [Shigley's Mechanical Engineering Design], 1002, McGraw-Hill, 8 ed. (January 2006).

- [10] Yong, Y. K. and Lu, T.-F., "Comparison of circular flexure hinge design equations and the derivation of empirical stiffness formulations," in [2009 IEEE/ASME International Conference on Advanced Intelligent Mechatronics], IEEE (July 2009).
- [11] Schotborgh, W., Kokkeler, F., Tragter, H., and Van Houten, F., "Dimensionless design graphs for flexure elements and a comparison between three flexure elements," *Precision Engineering* **29**, 41–47 (01 2005).
- [12] Schindelin, J., Arganda-Carreras, I., Frise, E., Kaynig, V., Longair, M., Pietzsch, T., Preibisch, S., Rueden, C., Saalfeld, S., Schmid, B., Tinevez, J.-Y., White, D. J., Hartenstein, V., Eliceiri, K., Tomancak, P., and Cardona, A., "Fiji: an open-source platform for biological-image analysis," *Nature Methods* 9, 676–682 (jun 2012).
- [13] Rasband, W. S., [ImageJ], U. S. National Institutes of Health (1997-2018). https://imagej.nih.gov/ij/.